Virology 529 (2019) 43–56

Contents lists available at ScienceDirect

Virology

journal homepage: www.elsevier.com/locate/virology

Impact of dynamin 2 on adenovirus nuclear entry

Ji Sun Lee, Ashrafali M. Ismail, Jeong Yoon Lee[1], Xiaohong Zhou, Emma C. Materne, James Chodosh, Jaya Rajaiya*

Howe Laboratory, Mass Eye and Ear, Department of Ophthalmology, Harvard Medical School, Boston, MA 02114, USA

ARTICLE INFO

Keywords:
Adenovirus
Cytokines
Dynamin 2
Microtubule organizing center
Microtubules
Nucleoporin
Viral trafficking

ABSTRACT

The large GTPase dynamin 2 controls both endosomal fission and microtubule acetylation. Here we report that dynamin 2 alters microtubules and regulates the trafficking of human adenovirus type 37. Dynamin 2 knockdown by siRNA in infected cells resulted in accumulation of acetylated tubulin, repositioning of microtubule organizing centers (MTOCs) closer to cell nuclei, increased virus in the cytosol (with a compensatory decrease in endosomal virus), reduced proinflammatory cytokine induction, and increased binding of virus to the nucleoporin, Nup358. These events led to increased viral DNA nuclear entry and viral replication. Overexpression of dynamin 2 generated opposite effects. Therefore, dynamin 2 inhibits adenovirus replication and promotes innate immune responses by the infected cell. MTOC transposition in dynamin 2 knockdown promotes a closer association with nuclear pore complexes to facilitate viral DNA delivery. Dynamin 2 plays a key role in adenoviral trafficking and influences host responses to infection.

1. Introduction

Dynamins belong to a super-family of large GTPases that includes dynamin-like proteins. Three types of dynamin are well characterized. Dynamin 1 is found in neurons and brain, dynamin 2 is ubiquitously present, and dynamin 3 is found in testis, lung and heart. Dynamin 2 was first identified as a microtubule binding protein (Shpetner and Vallee, 1989), and later confirmed to be a GTPase activated by microtubules (Shpetner and Vallee, 1992). However, less attention was given to dynamin's microtubule-associated function after the identification of a critical role for dynamin in vesicle fission in endocytosis. Dynamin 2 has been shown necessary for the entry of several viruses, including hepatitis E virus (Holla et al., 2015), Ebola virus (Aleksandrowicz et al., 2011; Mulherkar et al., 2011), dengue 2 virus (Shrivastava et al., 2011), influenza A virus (de Vries et al., 2011), and HIV (Carter et al., 2011). All these reports focused on the GTPase function of dynamin 2 in fission and endocytosis. However, the role of dynamin 2 in microtubule stability and its impact on viral trafficking have not been addressed.

Microtubules form the skeletons of cells and control the positioning of many organelles within the cell, such as the Golgi apparatus, lysosomes, and endosomes. The cell nucleus is often found close to the microtubule organizing center (MTOC), also known as the centrosome (Thyberg and Moskalewski, 1999). Microtubules have inherent polarity, with a slow growing minus end towards the center of the cell, and a fast growing plus end towards the cell periphery (Mitchison and Kirschner, 1984a, 1984b; Salmon et al., 1984), referred to as the dynamic instability of growth. Adenovirions must reach the nuclei of infected cells to replicate and produce progeny, and was long been known to associate with microtubules (Dales and Chardonnet, 1973; Miles et al., 1980). Human adenoviruses (HAdV) cause upper and lower respiratory, gastrointestinal, ocular, and urinary tract infections, and are classified into seven species (A-G) with 90 unique genotypes in GenBank. In HeLa and TC7 cells, movement of cytosolic HAdV-C2 towards the nucleus depended on intact, but not dynamic microtubules (Suomalainen et al., 1999). Moreover, the endosomal escape-defective mutant adenovirus ts1 was shown not to reach the perinuclear MTOC. Rather, only wild type virus that escaped the endosome and became cytosolic reached the MTOC (Suomalainen et al., 1999). HAdV-C2 was shown to associate with MTOC up to 5 h post-infection (Bailey et al., 2003), suggesting that adenovirus association with MTOC may be prerequisite to adenovirus DNA delivery to the nucleus. However, to date there is no compelling evidence connecting MTOC localization near the nuclear membrane with a physical interaction between virions and the nuclear pore complex. Approximately 2000 nuclear pore complexes, each consisting of ~30 different proteins (nucleoporins, Nups), are distributed on the nuclear envelope. Nucleoporins act as gatekeepers for the active import and export of large molecules between the nucleus and cytoplasm. One particular nucleoporin, Nup358,

* Corresponding author.
E-mail address: jaya_rajaiya@meei.harvard.edu (J. Rajaiya).
[1] Present address: Molecular Virology Laboratory, Korea Zoonosis Research Institute, Jeonbuk National University, Iksan, Republic of Korea.

https://doi.org/10.1016/j.virol.2019.01.008
Received 9 August 2018; Received in revised form 6 January 2019; Accepted 7 January 2019
Available online 10 January 2019
0042-6822/ © 2019 Elsevier Inc. This article is made available under the Elsevier license (http://creativecommons.org/licenses/by-nc-nd/4.0/).

localizes to the cytoplasmic side of the NPC and has been implicated in both SUMOylation and kinetochore-microtubule association (Asally et al., 2011; Joseph et al., 2002; Pichler et al., 2002; Salina et al., 2003).

Dynamin 2 regulates dynamic instability of microtubules, which is essential for organelle motility. Acetylation of tubulin has been reported during entry and trafficking of several viruses, including adenovirus (Belin and Boulanger, 1985; Frampton et al., 2010; Husain and Harrod, 2011; Kelkar et al., 2004; Valenzuela-Fernandez et al., 2005; Zhong et al., 2014). Herein we present a novel function for dynamin 2 in trafficking of HAdV-D37 during the initial phases of infection. We found that dynamin 2 knockdown in keratocytes led to increased acetylated tubulin, repositioning of MTOCs closer to cell nuclei, greater viral DNA entry to cell nuclei, and increased viral replication. Importantly, dynamin 2 knockdown prior to viral infection was also associated with reduced cytokine expression, as compared to cells treated with scRNA or in which dynamin 2 was overexpressed. Transfection of the dynamin 2 mutant Δ551-553, earlier reported to cause accumulation of acetylated tubulin (Tanabe and Takei, 2009), and implicated in Charcot-Marie-Tooth disease (Zuchner et al., 2005), increased viral gene expression as compared to wild type dynamin 2, as did Δ746-786, lacking the microtubule binding site (Hamao et al., 2009).

2. Results

2.1. Viral trafficking is pH independent, but microtubule polymerization dependent

Endosomal acidification during intracellular trafficking is critical for many viruses (Giovanni et al., 2000; Lee et al., 2011; Shtanko et al., 2014; Wenzel et al., 2011). However, there are reports that trafficking of viruses can be independent of endosomal acidification in certain cell types (Boritz et al., 1999; Haspot et al., 2012; Kamiyama et al., 2011). In order to test whether trafficking of HAdV-D37, a severe eye pathogen, is dependent on endosomal acidification in primary human keratocytes, derived from deceased corneal donors, we pretreated cells with varying amounts of bafilomycin A, an endosomal acidification repressor, and infected the cells with virus. Keratocytes pretreated with bafilomycin A prior to infection showed no reduction in viral gene expression even at 500 nM for up to 2 h post infection (pi) (Fig. 1A and data not shown), with E1A expression levels similar to virus and DMSO control groups. These results suggest that HAdV-D37 entry in keratocytes is independent of endosomal acidification, in confirmation of prior work suggesting that HAdV-D37 entry in keratocytes occurs via caveosomes (Yousuf et al., 2013), a process not known to require acidification.

We then applied cytochalasin D, a potent inhibitor of actin polymerization, as a pretreatment prior to infection. Cells pretreated with cytochalasin D showed a dose-sensitive reduction in viral gene expression (Fig. 1B) as compared to virus only and DMSO treated, virus infected cells, but viral gene expression was still evident even at a concentration of 2 μM. In comparison, pretreatment with the microtubule polymerization inhibitor, nocodazole, at either 10 μM or 30 μM, completely abrogated HAdV-D37 gene expression in keratocytes as compared to controls (Fig. 1C). We further examined the effect of nocodazole on viral entry by confocal microscopy with Cy3-labeled virions (Fig. 1D). Cells infected after DMSO treatment showed intracellular virions (Fig. 1D, panel 1), whereas virions were not evident within nocodazole pretreated cells (Fig. 1D, panel 2). These data appeared in agreement with viral gene expression data in Fig. 1C. Because of this observed effect of nocodazole, an inhibitor of microtubule polymerization, we next turned to examination of dynamin 2, a protein previously implicated in endocytosis of viruses, and known to bind and modify microtubules.

2.2. Dynamin 2 negatively regulates viral gene expression

Dynamin 2 has been reported to play a role in pinching of vesicles from the plasma membrane during endocytosis, (Ferguson and De Camilli, 2012) and in microtubule and actin skeleton dynamics (Gonzalez-Jamett et al., 2013). To investigate a possible effect of dynamin 2 on viral entry and trafficking of adenovirus, we treated primary keratocytes with siRNA against dynamin 2 and then infected with HAdV-D37 for 2 h. Measurement by Western blot (Fig. 1E, upper panel) and qRT-PCR (Fig. 1E, lower panel) each indicated knockdown. We included AP2A1 as a negative control for dynamin 2 knockdown. Quantitative RT-PCR for E1A gene expression, a surrogate marker of viral infection, using the same pool of total RNA as in Fig. 1E, indicated that dynamin 2 siRNA knockdown (siDNM2) enhanced viral gene expression by ~4-fold as compared to control, scrambled (sc)RNA transfection (Fig. 1F). We then questioned the consequence of overexpression of a dynamin 2 fusion protein (OE-DNM2) in viral gene expression. Successful overexpression of dynamin 2 was shown by Western blot (arrow, Fig. 1G, upper panel) and qRT-PCR (Fig. 1G, lower panel). Viral E1A expression was reduced by ~50% in cells with overexpressed dynamin 2 as compared to empty vector control (EV), (Fig. 1H). These results strongly suggest that dynamin 2 negatively regulates adenovirus entry and/or trafficking in human keratocytes.

2.3. Tubulin acetylation upon dynamin 2 knockdown is associated with enhanced adenovirus trafficking

Adenoviral trafficking is reported to require intact microtubules (Leopold et al., 2000), and mutations in dynamin 2 increase acetylation and accumulation of stable microtubules (Tanabe and Takei, 2009). As our results above indicated an increase in viral gene expression upon dynamin 2 knockdown, we further investigated whether changes in microtubule stability contributed to increased viral trafficking. Western blot analysis showed an increase in acetylated tubulin upon viral infection. This effect on tubulin acetylation was reduced by dynamin 2 overexpression (Fig. 2A), and increased by pretreatment with siDNM2 (Fig. 2B). Confocal microscopy of mock infected cells after pretreatment with siDNM2 clearly shows a more marked increase in tubulin accumulation near the perinuclear regions (arrow, Fig. 2C. row 2), in comparison to the other treatment groups. Treatment of nonenveloped virions with Cy3 dye labels external capsid proteins. At 1 h pi, confocal analysis showed Cy3-labeled virions in the same regions where accumulation of acetylated tubulin was observed, when cells were knocked down for dynamin 2 (Fig. 2C, rows 3 and 4). In contrast, in cells infected after overexpression of dynamin 2, scRNA, or empty vector, acetylated tubulin and Cy3-labeled virions appeared more dispersed with comparatively less accumulation near the perinuclear regions.

2.4. Dynamin 2 knockdown increases nuclear targeting of virus

EdU labeling of DNA by click chemistry can enable visualization of viral DNA by microscopy (Wang et al., 2013). Using EdU labeling of HAdV-D37 to visualize the viral DNA with simultaneous labeling of acetylated tubulin, we next sought to determine whether increased virus in the perinuclear region of cells knocked down for dynamin 2 was associated with increased viral DNA nuclear entry. Viral infection induced tubulin acetylation (red) similar to that observed in Fig. 2. Confocal analysis at both 1 and 2 h pi appeared to show more viral DNA (green) in the nuclei of siRNA treated cells, as shown by highlighted circles around each nucleus (Fig. 3A, d-1 and h-1), with comparatively less viral DNA in nuclei of the cells treated with scRNA (Fig. 3A, c-1, g-1) or in cells transfected with empty vector (Fig. 3A, a-1,e-1), or in cells where dynamin 2 was overexpressed (Fig. 3A, b-1, f-1). Quantification by ImageJ analysis of EdU fluorescence, restricted to images from the nuclear stack as described in the Methods, showed significantly greater signal in the nuclei of HAdV-D37 infected cells pretreated with

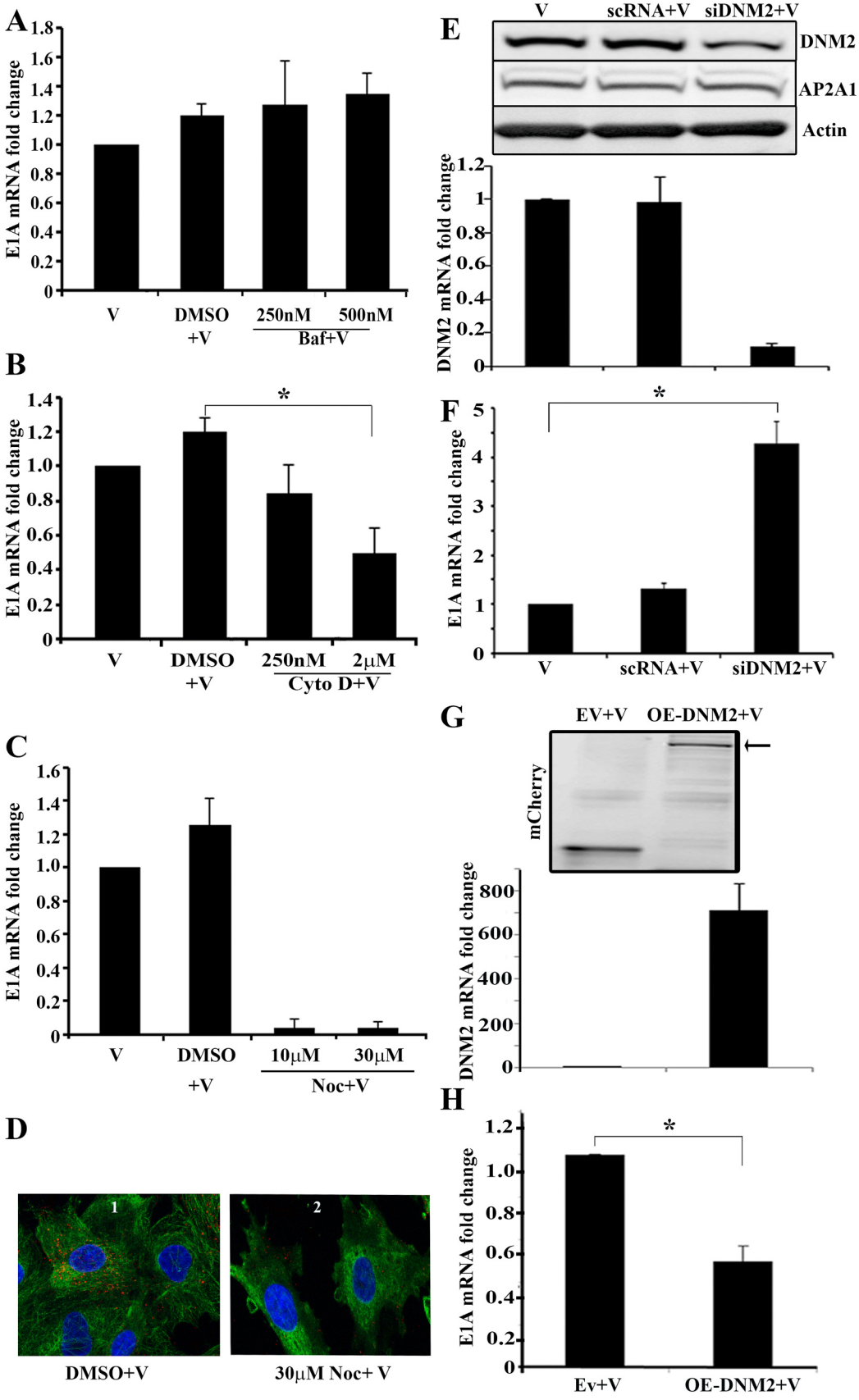

(caption on next page)

Fig. 1. Dynamin 2 negatively regulates viral gene expression. A. E1A expression at 2 h pi as measured after virus infection alone (V), or infection following bafilomycin A pretreatment (Baf + V) at 250 nM or 500 nM, and in the solvent control (DMSO + V). **B.** Effect on E1A mRNA expression of pretreatment with cytochalasin D prior to virus infection (Cyto D + V) at 250 nM or 2 μM; solvent control (DMSO + V), virus alone (V); 2 h pi (DMSO + V vs. Cyto D + V 2 μM; *$p < 0.05$, ANOVA). **C.** Effect on E1A mRNA expression of pretreatment with nocodazole prior to viral infection (Noc + V) at 10 μM or 30 μM, virus alone (V), and DMSO control (DMSO + V). **D.** Confocal microscopy representation of viral entry at 2 h pi in the presence of solvent control (panel 1, DMSO + V) or 30 μM nocodazole (panel 2, Noc + V). Cy3 labeled HAdV-D37 (red), anti-α tubulin staining (green). **E.** Western blot showing protein expression levels in keratocytes after dynamin 2 (DNM2) knockdown: mock transfected and virus infected (V), scRNA transfected and virus infected (scRNA + V), siDNM2 transfection prior to viral infection (siDNM2 + V). Western blot for α-AP2A1, an adaptor protein shown as negative control for specificity of DNM2 knockdown. Actin blot shows load control. Dynamin 2 mRNA expression levels by qRT-PCR are represented in bar graph just below. **F.** Early gene expression (E1A) as measured by qRT-PCR from same RNA pool as in E: virus alone (V), scrambled RNA (scRNA + V), dynamin 2 knockdown, virus infected cells (siDNM2 + V) (*$p < 0.001$, ANOVA). **G.** Western blot shows expression of mCherry in empty vector prior to virus infection (EV + V) and mCherry-dynamin 2 (arrow) prior to virus infection (OE-DNM2 + V). The bar graph just below shows mRNA expression of dynamin 2. **H.** E1A mRNA expression as measured in cells after dynamin 2 vector pretreatment, performed on same RNA pool from G (*$p = 0.01$, Students *t*-test). Error bars represent standard deviation of the mean. Each experiment was repeated at least 5 times with similar results.

dynamin 2 siRNA ($p < 0.0001$) (Fig. 3B).

In addition to modifying microtubules, dynamin 2 also regulates endosomal fission. To consider the possibility that increased nuclear entry in dynamin 2 knockdown was due to an effect of dynamin 2 on endosomal fission affecting viral endocytosis, we next examined the relative amount of viral DNA in cells at 30 min after infection at 37 °C, measured by conventional PCR at three separate regions of the genome. As shown, we did not observe differences in the amount of viral DNA in any pretreated group by PCR (Fig. 3C) or by quantitative PCR (Fig. 3D), inconsistent with a role for dynamin 2 in viral endocytosis in these cells, and suggesting that the effect of dynamin 2 on viral trafficking occurs downstream of membrane penetration.

Adenovirus DNA replication occurs in cell nuclei. As shown above, the extent of cellular entry was not appreciably affected by dynamin 2 knockdown, although nuclear entry of viral DNA was clearly increased. To determine whether increased viral DNA in cell nuclei in dynamin 2 knockdown leads to increased viral production, we infected cells after dynamin 2 knockdown, dynamin 2 overexpression, or their controls (scRNA and empty vector, respectively), and performed a viral titration assay from culture supernatants taken at 12 h pi. As shown in

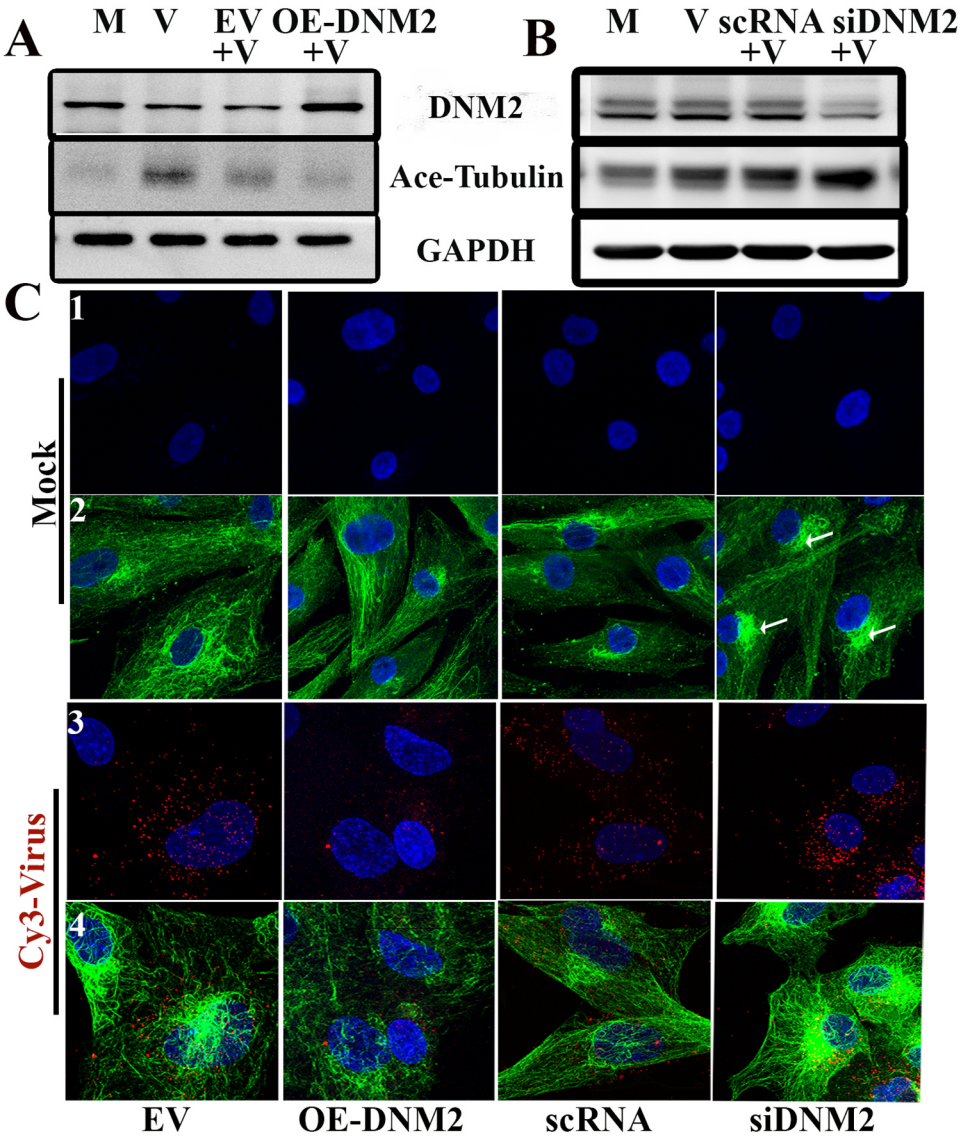

Fig. 2. Tubulin acetylation is associated with enhanced adenovirus trafficking. A. Western blot for dynamin 2, acetylated tubulin, and GAPDH after mock infection (M), virus infection (V), empty vector transfection prior to virus infection (EV + V), and dynamin 2 vector transfection prior to infection (OE-DNM2 + V). Blots were cut at the appropriate sizes and probed with specific antibodies. **B.** Western blot for dynamin 2 protein, acetylated tubulin, and GAPDH in cells after treatment with scRNA or dynamin 2 siRNA prior to viral infection (scRNA + V, siRNA + V, respectively). **C.** Confocal microscopy of mock and Cy3-labeled (red) virus infected cells, 1 h pi, stained for acetylated tubulin (green). Mock infected and virus infected cells both show increased perinuclear acetylated tubulin when knocked down for dynamin 2 (row 2, right hand column, arrows, and row 4, right hand column). Virions in cells knocked down for dynamin 2 appear to accumulate in the perinuclear region at 1 h pi. Each experiment was repeated at least 5 times with similar results.

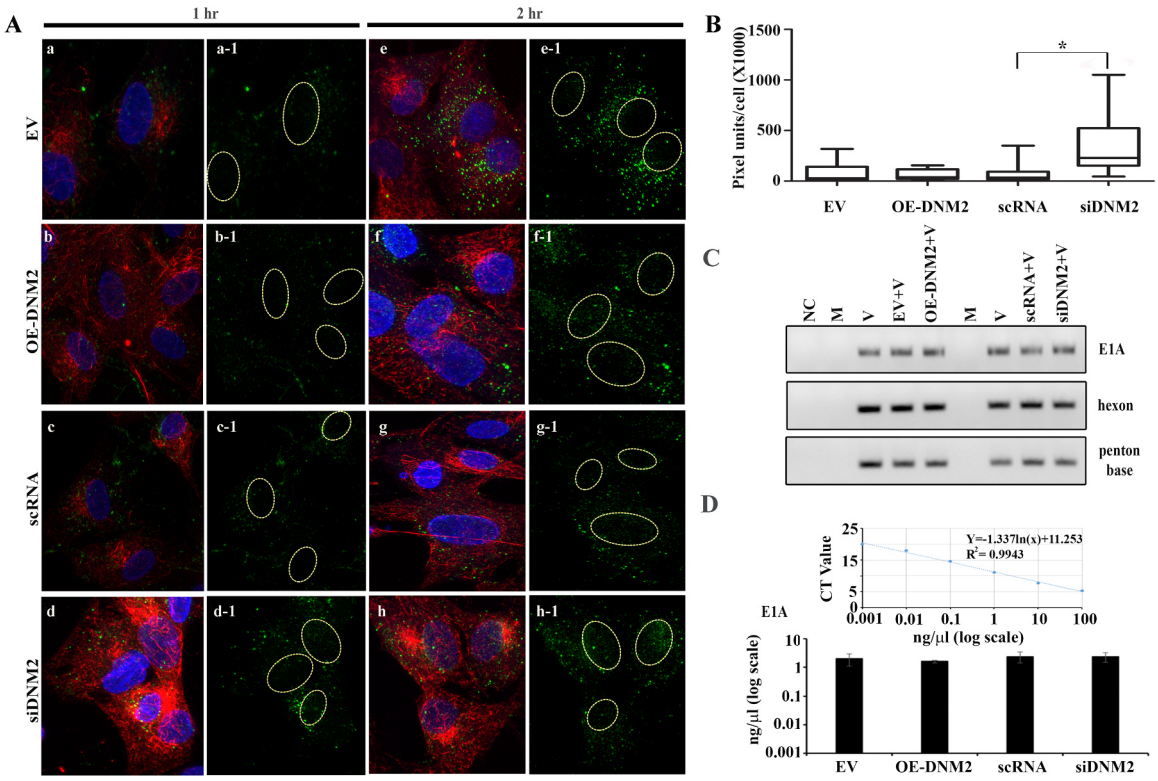

Fig. 3. Dynamin 2 knockdown increases nuclear targeting of adenovirus. A. Acetylated tubulin (red) after infection with EdU labeled virus (green) at 1 and 2 h pi, after empty vector transfection prior to virus infection (EV), dynamin 2 vector transfection prior to infection (OE-DNM2), pretreatment with scRNA or dynamin 2 siRNA (siDNM2). DAPI staining (blue) of nuclei utilized to outline blue-free images (a-1 through h-1), in order to better visualize virions in cell nuclei. **B.** Quantification of green fluorescence (pixel units) from A (2 h pi) within ovals outlines (nuclei) as measured using ImageJ and shown graphically in box plot (*p < 0.0001, Kruskal-Wallis). Data was obtained from 20 cells per experimental group in three experimental replicates. **C.** PCR for HAdV-D37 E1A, hexon and penton base genomic DNA measured to show relative levels of viral entry at 30 min pi. **D.** Quantitative real-time PCR for E1A DNA under the same experimental conditions. Upper graph shows the standard curve for E1A DNA. Lower graph demonstrates no statistical difference between experimental groups Each experiment was repeated at least 3 times with similar results.

Supplemental Table 1, viruses grown in cells knocked down for dynamin 2 replicated to a titer roughly 7-fold higher than scRNA control (6.7×10^5 vs. 1×10^5 $TCID_{50}$, respectively), while viral replication in OE-DNM2 treated cells was only 0.4 fold of its control, EV treated cells (1.7×10^4 vs. 4×10^4 $TCID_{50}$, respectively). Recognizing that transfections of siRNA and the dynamin 2 construct are not identical processes, titers from 12 h pi supernatants were about 40-fold higher titer in siDNM2 cells as compared to cells in which dynamin 2 was overexpressed (6.7×10^5 vs. 1.7×10^4 $TCID_{50}$, respectively). Taken together with the data in Fig. 3, these results suggest that the effect of dynamin 2 knockdown on viral replication is due to increased viral trafficking to the nucleus rather than an effect on cellular entry.

2.5. Dynamin 2 knockdown increases the abundance of virus in the cytosol

Earlier reports indicated that various viruses use microtubules to access the nucleus (Leopold et al., 1998, 2000; Nakano and Greber, 2000; Suomalainen et al., 1999), specifically that stable, non-dynamic microtubules enhance nuclear-directed viral trafficking (Mabit et al., 2002; Naranatt et al., 2005; Suomalainen et al., 2001). Based on the data above, we questioned whether the viruses that enter cells knocked down for dynamin 2 are contained within endosomes or found free in the cytosol. We used the recently introduced streptolysin O (SLO) assay (Suomalainen et al., 2013) that enables visualization and differentiation of endosome-trapped versus cytosolic virions (Fig. 4A). Because SLO permeabilizes only plasma membranes and not endosomal membranes, fluorescently tagged antibodies will not pass into endosomes of SLO treated cells. Cy3-labeled virions within endosomes retain their red fluorescence, while virions in the cytosol appear yellow upon binding to anti-Cy3 antibody with a green chromophore. As a control to ensure that our SLO assay is indeed specific to differentiate cytosolic from endosomal virus, cells were also treated with Triton X-100, which permeabilizes both plasma and endosomal membranes, thus allowing anti-Cy3 antibody to stain both cytosolic and endosomal viruses. Further, antibody against the Golgi marker GM-130 to show that the various transfections performed in our analyses do not affect the relative permeability to any antibody in the subsequent SLO assay (Fig. 4B panel 2–4). Virus appeared to be predominantly endosomal (red) in cells pretreated with either the empty vector control or those pretreated with the dynamin 2 expressing vector (Fig. 4C, right panels 1 and 2, respectively). In contrast cells pretreated with siDNM2 showed predominantly cytosolic virions (yellow; Fig. 4C, right panel 4) in comparison to scRNA pretreated cells, (Fig. 4C, right panel 3), in which virions were mostly within endosomes (red). As predicted for the SLO control group, in which cells were treated with 0.5% Triton X-100 but not SLO, virions appeared consistently yellow in color (Fig. 4C, left panel 1–4).

As a confirmation of our SLO analyses, in which dynamin 2 knockdown increased the localization of virions in the cytosol, we performed ultrastructural studies to identify cellular loci of HAdV-D37 under similar conditions. The microscopy sections shown demonstrate the localization of virions in endosomes (arrows) in cells treated with either empty vector or with a vector expressing dynamin 2 (Fig. 5A, left column). Alternatively, while endosomal virus was observed in scRNA pretreated cells (arrows; Fig. 5A, top right), the virions in cells knocked down for dynamin 2 appeared to be mostly in the cytosol (Fig. 5A, bottom right). Virions found in endosomes and in the cytosol were then quantified and the proportions compared across experimental

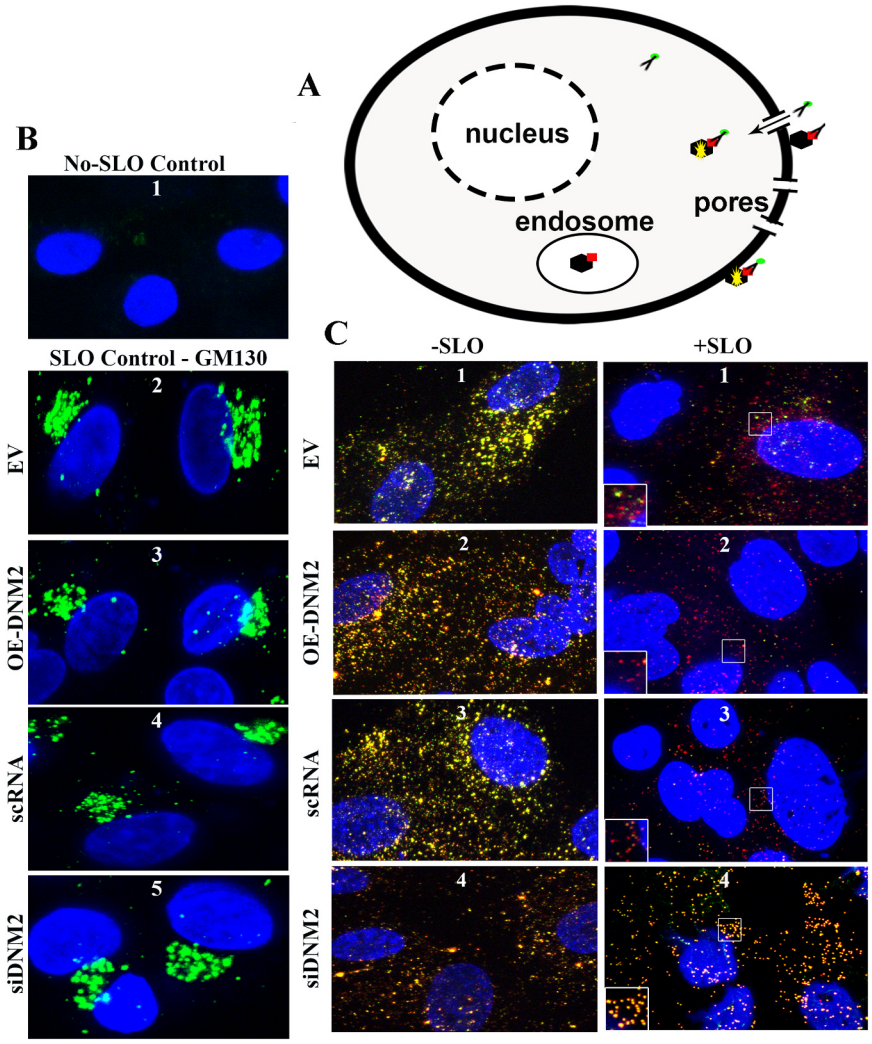

Fig. 4. Dynamin 2 knockdown increases virions in the cytosol relative to the endosome. A. Modified schematic of SLO assay (Suomalainen et al., 2013). In this assay, SLO permeabilizes only cell membranes and not endosomal membranes, so that Cy3-labeled virions within endosomes appear red, while virions in the cytosol appear yellow upon binding to anti-Cy3 antibody with a green chromophore. **B.** Streptolysin O (SLO)-penetration assay performed 1 h pi. Panel 1 shows the no-SLO control, where there is no staining for GM-130, indicating absence of antibody penetration. Panels 2–5 show equivalent staining for GM130 (green), indicating that the transfections did not affect pore formation by SLO. **C.** SLO assay performed in cells transfected prior to viral infection with empty vector (EV), dynamin 2 overexpression construct (OE-DNM2), scRNA, or siRNA (siDNM2). In SLO treated groups (+SLO), virions in endosomes appear red, while virions in cytosol appear yellow. As a control, left panel shows same groups treated with triton X100 without SLO (–SLO), and thus virions in both cytosol and endosomes appear yellow. Each experiment was repeated at least 3 times with similar results.

conditions for ten cells each. In cells pretreated with siDNM2, 15.9% of virions were identified in endosomes, compared to 76–84.3% in the other 3 experimental conditions (data not shown).

The route of trafficking has been implicated in differential innate immune responses as evident in differences in cytokine expression by cells infected with different HAdVs (Teigler et al., 2014). We next performed cytokine array analyses on cell supernatants after pretreatment with either empty vector versus dynamin 2 overexpression, or scRNA versus siDNM2, prior to infection (representative blots: Fig. 5B). Overexpression of dynamin 2 prior to viral infection led to statistically significant changes (increases) in only 2 of the 10 cytokines detected, specifically, CXCL10 and CXCL8 (Fig. 5C). In contrast, siDNM2 pretreatment led to statistically significant reductions in 6 out of the 10 detected cytokines ($p < 0.05$). These results connect virus localization and cytokine expression by the infected cells, consistent with the findings of Teigler and coworkers (Teigler et al., 2014).

We have previously shown that Src acts as a central signaling node in adenovirus infected keratocytes, impacting diverse functions such as viral replication and host cytokine expression (Natarajan et al., 2003; Rajaiya et al., 2009, 2015; Xiao and Chodosh, 2005; Yousuf et al., 2013). Src-mediated phosphorylation of dynamin 2 was previously reported to be essential to scission of endothelial cell caveolae (Shajahan et al., 2004). However, the data we present above suggests the impact of dynamin 2 in HAdV-D37 infection is on intracellular trafficking rather than cellular entry. We also examined Src phosphorylation in relation to the same four experimental manipulations of dynamin 2 utilized above. Upon siRNA pretreatment, Src phosphorylation in infected cell lysates was increased as compared to scRNA transfected cells (Supplemental Fig. 1A, left panel). When dynamin 2 was overexpressed, Src phosphorylation was reduced as compared to empty vector transfected cells (Supplemental Fig. 1A, right panel). These data as quantified in Supplemental Fig. 1B, suggest an inhibitory role for dynamin 2 on Src activation in infected cells, and are consistent with data above showing that dynamin 2 knockdown increases cytokine expression by infected cells.

2.6. Dynamin 2 regulates MTOC localization

The microtubule network nucleates at and radiates from the MTOC, also known as the centrosome. Suomalainen and colleagues previously determined that adenoviruses in the cytosol accumulated near the MTOC for nuclear import, while viruses within endosomes did not (Suomalainen et al., 1999). Other investigators studying adenovirus infections also observed the accumulation of adenoviruses near the MTOC (Bailey et al., 2003). Our confocal microscopy data suggested that microtubule acetylation and rearrangement in adenovirus infection are increased in dynamin 2 knockdown cells (Fig. 2C). Collectively, these data encouraged us to examine the localization of MTOC upon adenovirus infection in cells knocked down for dynamin 2, with similar controls as in the experiments above. MTOCs are rich in three major proteins: pericentrin, γ-tubulin, and centrin 2. We applied an antibody against pericentrin as a marker for MTOCs (Doxsey et al., 1994), and

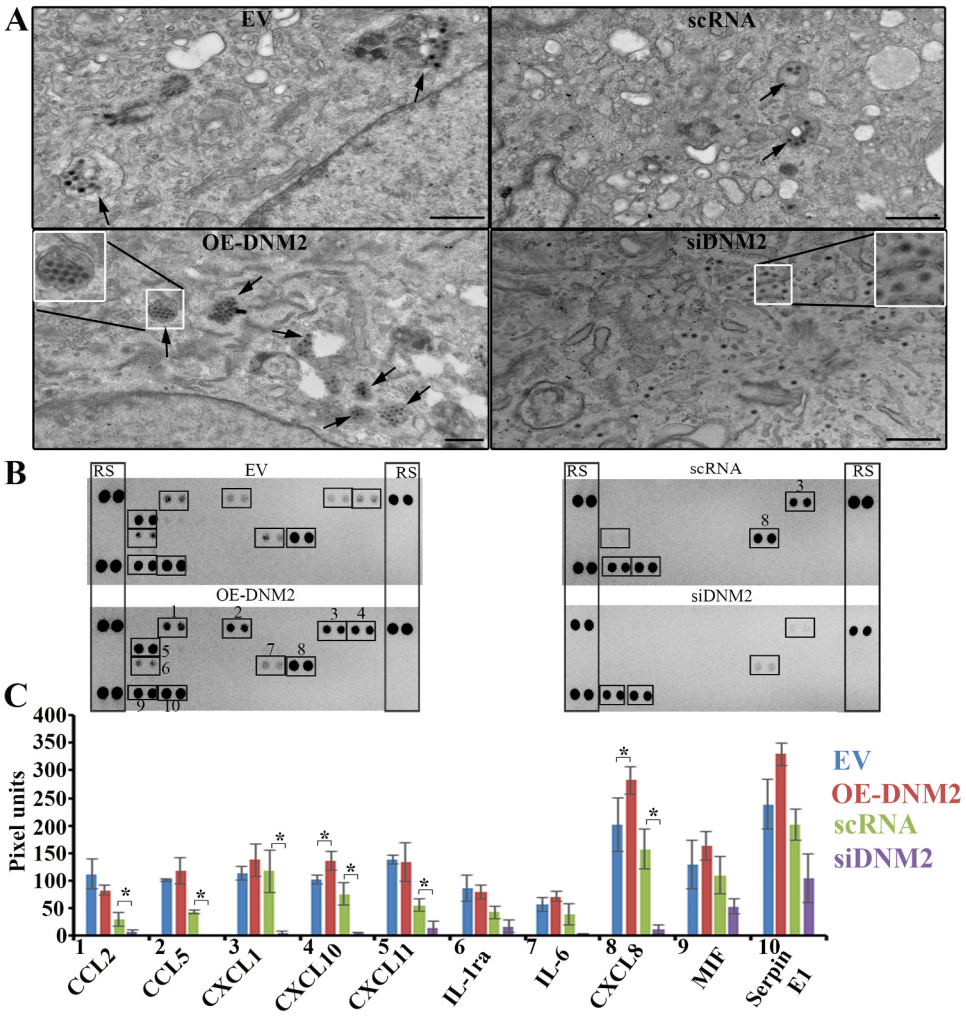

Fig. 5. Cytosolic virus is associated with reduced cytokine expression. A. HCF pretreated with EV, OE-DNM2, scRNA and siDNM2 were infected for at a MOI of 100, and ultrastructural images taken to locate virion distribution. Scale bar = 500 nm. Electron microscopy was performed three times with similar results. **B.** Cytokine arrays were performed on 500 µl of culture supernatants collected from each group after infection at MOI of 10 for 2.5 h. Reference spots (RS) were used as densitometric controls to quantify the mean spot pixel density. Detected cytokines included CCL2 (1), CCL5 (2), CXCL1 (3), CXCL10 (4), CXCL11 (5), IL-1ra (6), IL-6 (7), CXCL-8 (8), MIF (9) and Serpin E1 (10). **C.** Bar graph showing collated results from 3 separate assays. The means of densitometry measurements from three independent experiments were plotted, normalizing to reference spots. Error bars represent standard deviation of the means. * indicates those cytokines for which expression was reduced significantly by dynamin 2 siRNA, as compared to control scRNA (*$p < 0.05$, Students *t*-test).

measured the distance between the pericentrin fluorescent signal and the nearest nuclear membrane using LAS-X distance tools for a total of 100 cells per group, from randomly selected frames, in 3 separate experiments. By confocal microscopy (Fig. 6A), and as quantified by measuring distances between MTOCs and adjacent nuclei, we found that dynamin 2 knockdown led to smaller distances between MTOCs and adjacent cell nuclei than dynamin 2 overexpression ((Fig. 6B), * $p < 0.0001$). As confirmation, we then performed ultrastructural studies for MTOC localization for the same experimental groups (representative photomicrographs (3/group): Fig. 6C, and graphed (10/group): Fig. 6D). The mean distances between MTOCS and the nearest nuclear membranes in virus infected cells pretreated with empty vector, dynamin 2 overexpression, scRNA, or siDNM2 were 1.54 (standard deviation: 0.23), 4.04 (0.91), 1.58 (0.26), and 0.69 (0.08), respectively (Fig. 6D), $p < 0.05$, Students *t*-test for both comparisons.

Delivery of adenoviral DNA into the cell nucleus occurs through the nuclear pore complexes (NPC). Prior studies suggested that adenovirus capsids bind to the NPC protein Nup214 and kinesin-1 light-chain Klc1/2 (Strunze et al., 2011). Nup358, also known as Ran Binding Protein 2 (RanBP2), binds microtubules to the nuclear envelope, and also associates with Nup214. Nup358 mediates kinesin-driven disruption of the viral capsid, and promotes delivery of viral DNA through a compromised NPC, although this function of Nup358 was dispensable in HeLa cells (Cassany et al., 2015). By confocal microscopy, colocalization of virions with Nup358 varied along the nuclear membranes in all four experimental groups (Fig. 6E). However, Cy3-labeled virions co-localized to Nup358 only in keratocytes knocked down for dynamin 2 (Fig. 6E, insets). Similar experiments were performed using antibody to Nup214 and Nup98, but we did not observe any co-localization (data not shown).

2.7. Select dynamin 2 mutations enhance viral gene expression

Since our results strongly indicate that the dynamic instability of microtubules, as controlled by dynamin 2, is critical to viral trafficking, we decided to use dynamin 2 mutants shown previously to be defective in endocytosis and/or microtubule binding. Dynamin 2 has five characteristic domains. The GTPase domain resides at the N terminus. Adjacent are the Pleckstrin homology (PH) domain, a GTPase effector domain (GED) and a proline rich (PRD) C terminus domain (Fig. 7A). We used K44A, a GTPase mutant previously shown to block endocytosis (Al-Hasani et al., 1998), Δ551-553, with a mutation in the PH domain earlier shown to cause Charcot-Marie-Tooth disease, and which was shown to induce increased tubulin acetylation (Tanabe and Takei, 2009), and Δ746-786, which deletes amino acids at the PRD that physically bind microtubules (Hamao et al., 2009). After successful transfection, as shown by Western blot (Fig. 7B), cells were infected with adenovirus for 2 h, and E1A gene expression was measured as a surrogate marker for successful viral trafficking to cell nuclei. As shown in Fig. 7C, compared to wild type dynamin 2, both Δ551-553 and Δ746-786 appeared to enhance viral gene expression, but only the putative microtubule binding deficient Δ746-786 induced a statistically significant change in E1A expression (Wt versus Δ746-786, $p < 0.05$, Tukey test). Viral gene expression in K44A transfected cells was not statistically different from wild type (Fig. 7C), indicating that GTPase activity is not crucial for viral trafficking. These data appear to confirm

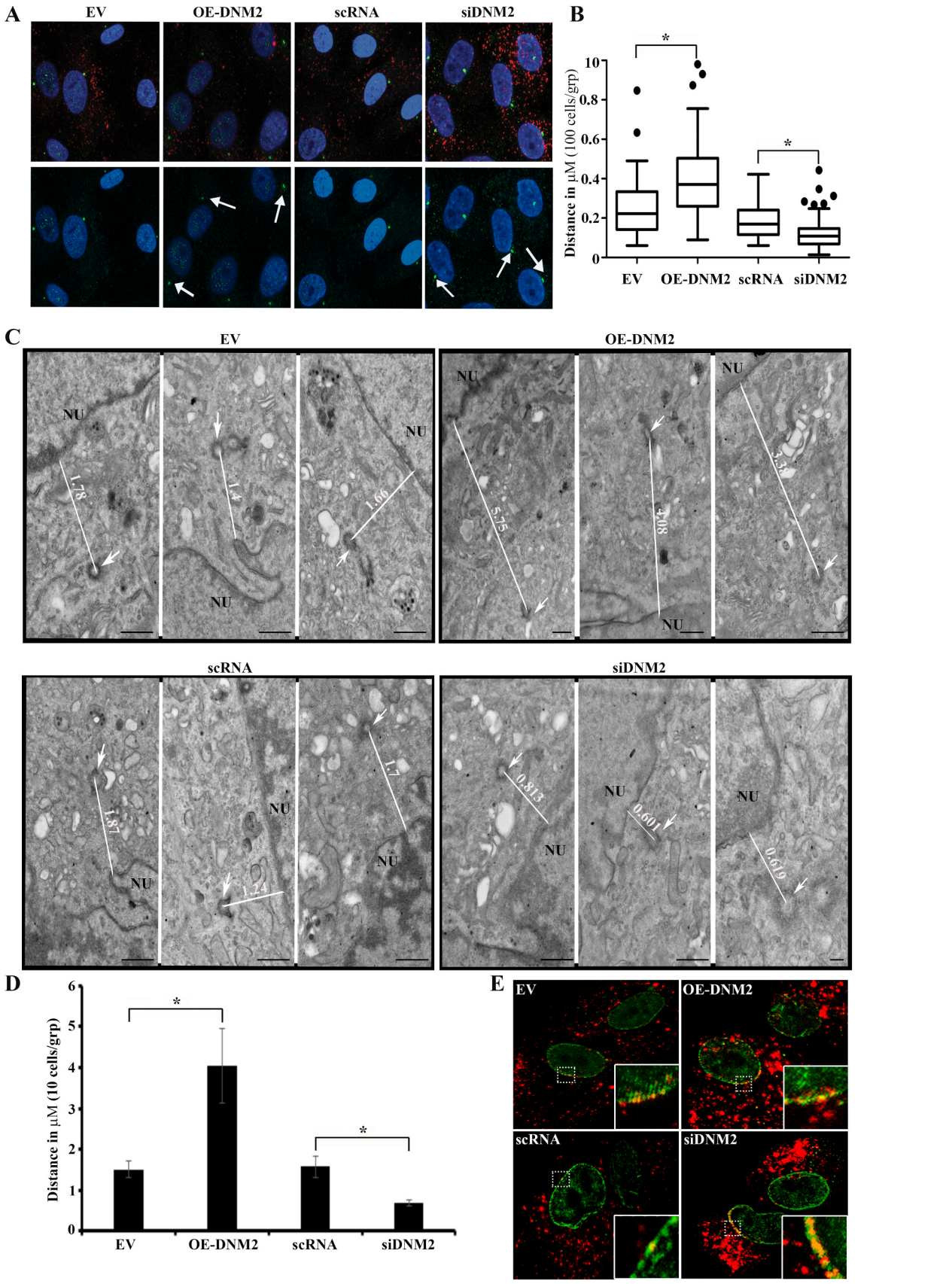

(caption on next page)

Fig. 6. Dynamin 2 regulates MTOC localization. A. Confocal microscopy of cells pretreated with empty vector (EV), dynamin 2 expressing vector (OE-DNM2), scRNA, or dynamin 2 siRNA (siDNM2) and infected with Cy3-labeled HAdV-D37 (red) for 1 h, and stained with anti-pericentrin (green), and DAPI (blue). **B.** Distance from green signals (arrows) to the closest edge of adjacent nuclei (100 cells per experimental group in three experiments) was measured using Leica application suite X (LAS X, Leica Microsystems, Wetzlar, Germany), and graphed in boxplots (*p < 0.0001, Kruskal-Wallis). **C.** Transmission electron microscopy of infected keratocytes from same pretreatment groups, with 3 distinct images shown per group shown. NU: nucleus. Scale bar = 500 nm. **D.** Measurements taken from each microtubule organizing center to nearest nuclear membrane were performed on 10 cells per group by a masked observer. Data shown reflects means and standard deviation for each group (*p < 0.05, Students *t*-test). **E.** Confocal microscopy showing co-localization (yellow) of nuclear pore complex protein Nup358 (green), and Cy3-labeled HAdV-D37 (red), 2 h pi. Each experiment was performed three times with similar results.

our hypothesis that dynamin 2 function in primary keratocytes serves to inhibit viral trafficking through its effect on microtubule dynamics. A proposed model for the effect of dynamin 2 in keratocytes on microtubules, MTOCs, and viral trafficking is shown in Fig. 8.

3. Discussion

Understanding viral trafficking can lead to the development of novel therapies against infection (Shurtleff et al., 2012). Using the highly pathogenic HAdV-D37, we initiated studies of adenoviral trafficking in keratocytes to determine basic cellular mechanisms during infection that might be vulnerable to new therapeutic approaches. Our viral gene expression experiments performed with the chemical inhibitors bafilomycin A and nocodazole, respectively, suggested that viral trafficking was pH independent but microtubule dependent. Although dynamin 2 is best known as critical to the fission of endocytic vesicles (De Camilli et al., 1995; Takei et al., 1995), it was initially identified as a microtubule binding protein (Maeda et al., 1992; Scaife and Margolis, 1990; Shpetner and Vallee, 1992), and is now recognized to regulate the dynamic instability of microtubules (Shpetner and Vallee, 1989; Tanabe and Takei, 2009). Microtubules have been previously shown to mediate adenoviral trafficking (Wang et al., 2018). Therefore, we sought to determine whether manipulation of dynamin 2 might impact microtubules and consequently influence HAdV-D37 trafficking and replication. Remarkably, dynamin 2 knockdown increased viral gene expression (a surrogate marker for successful viral trafficking to cell nuclei), while dynamin 2 overexpression reduced viral gene expression. These experimental results differ from previous reports that showed a positive influence of dynamin 2 on viral entry (Aleksandrowicz et al., 2011; Carter et al., 2011; de Vries et al., 2011; Holla et al., 2015; Mulherkar et al., 2011; Shrivastava et al., 2011). We did not observe an effect of dynamin 2 on endocytosis of HAdV-D37, but rather an indirect effect on trafficking associated with its modulation of microtubules. We previously showed that HAdV-C2 does not enter corneal cells (Yousuf et al., 2013). The observed effect of dynamin 2 shown herein may reflect a cell-specific role.

More than 20 mutations in dynamin 2 have been identified in association with hereditary neuromuscular diseases (Gonzalez-Jamett et al., 2013). Mutations in dynamin 2 contribute to acetylation and accumulation of stable microtubules that we speculated might impact viral transport (Tanabe and Takei, 2009). Using either siRNA or an overexpressing dynamin 2 construct, we showed that dynamin 2 negatively regulates the overall level of tubulin acetylation. Acetylated tubulin in cells knocked down for dynamin 2 also tended to accumulate adjacent to cell nuclei in both uninfected and infected keratocytes, and in infected cells this coincided with accumulations of viral capsid, and a quantifiable increase in the delivery of viral DNA to cell nuclei. This was not due to increased cellular entry of virus, as manipulation of dynamin 2 expression had no effect on the total amount of viral DNA in cells as assessed by quantitative PCR.

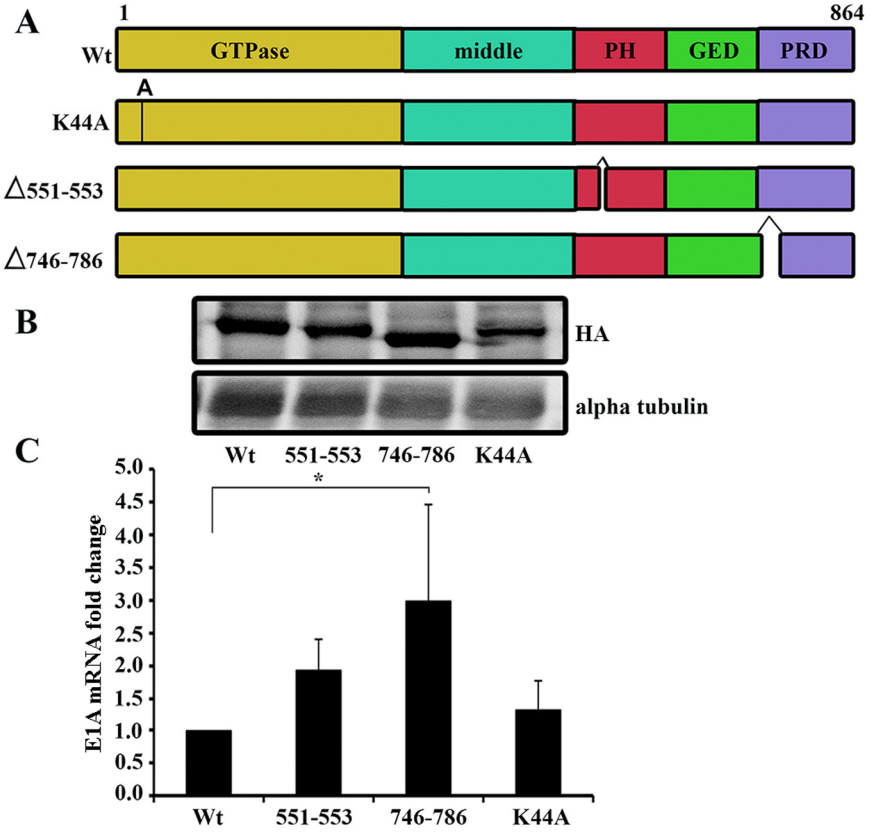

Fig. 7. Effect of dynamin 2 mutations on viral gene expression. A. Schematic presentations of dynamin 2 wild type and mutant clones. **B.** Western Blot for wild type (Wt), Δ551-553, and 746–786, with alpha tubulin load control. **C.** qRT-PCR for E1A mRNA expression with the same treatment groups as in A (*p < 0.05, ANOVA, with Tukey procedure). Experiments in both B and C were performed three times with similar results.

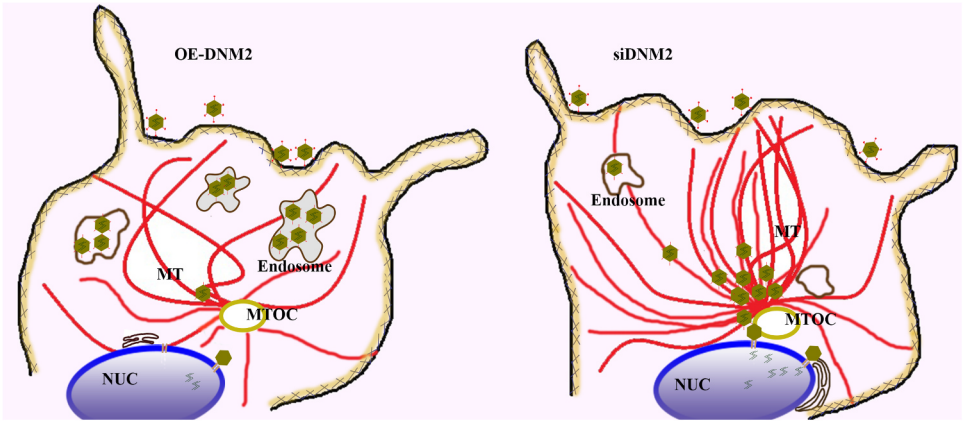

Fig. 8. Schematic of the role of dynamin 2 in viral trafficking. Our experiments in primary fibroblasts indicate that upon dynamin 2 overexpression (OE-DNM2), virions accumulate in endosomes, and hence are stalled from reaching the microtubule organizing center (MTOC) and nucleus (Nuc). Knockdown of dynamin 2 (siDNM2) localizes virions in the cytosol, with increased acetylation of microtubules (MT), and movement of MTOC closer to the nuclear membrane, thus enabling nuclear entry.

Prior studies of adenoviral entry into cells have focused almost entirely on clathrin-mediated endocytosis, with intracellular trafficking of virus-containing endosomes, pH mediated viral capsid disruption, and endosomal release at nuclear pores, and entry of viral DNA into cell nuclei (Nemerow, 2000). However, we recently showed that in keratocytes, HAdV-D37 but not HAdV-C2 utilized caveolin-1 for entry (Yousuf et al., 2013), consistent with prior work showing that entry and trafficking of adenoviruses is virus type specific (Teigler et al., 2014). We applied the streptolysin O assay (Suomalainen et al., 2013) to determine in keratocytes whether HAdV-D37 traffics predominantly via endosomes or through the cytosol, and to what degree this is controlled by dynamin 2. In untreated and control treated cells at 1 h pi, virions were predominantly endosomal. Endosomal virions were even more evident in the setting of dynamin 2 overexpression, possibly because dynamin 2 drives endosomal fission. However, in the setting of dynamin 2 knockdown, virions localized more to the cytosol. This observed differential between endosomal versus cytosolic virus was confirmed by transmission electron microscopy. However, what membrane modifications rendered virions to the cytosol in the setting of reduced dynamin 2 is unclear. We hypothesize however that virus in the cytosol better enables trafficking towards the nucleus via stable microtubules. It has also been suggested that endosomal virus is more inflammatory than virus in the cytosol (Teigler et al., 2014), perhaps because of endosome specific molecular pattern receptors such as Toll-like receptor 9 (Basner-Tschakarjan et al., 2006; Perreau et al., 2012). This is important also because robust innate immune responses to adenovirus infection have impeded progress in gene therapy using adenoviral vectors (Majhen et al., 2014). Using protein cytokine arrays, dynamin 2 expression was inversely correlated with proinflammatory cytokine expression. Furthermore, dynamin 2 expression was negatively correlated with activation of Src, a master signaling molecule shown previously to control proinflammatory gene expression in adenovirus infected keratocytes (Natarajan et al., 2003).

A specific role for dynamin 2 in MTOC reorganization has not been previously explored. Intact stable microtubules were previously shown to be necessary for adenoviral trafficking (Suomalainen et al., 1999). Adenovirus accumulates at the MTOC in experimentally enucleated cells (Bailey et al., 2003). Adenovirus accumulation at perinuclear MTOC facilitates binding of viral capsid to the nuclear pore complex for viral DNA delivery to the nucleus (Glotzer et al., 2001), however, precisely how virions transit from the MTOC to the nuclear envelope remains uncertain. In HeLa cells, adenovirus (HAdV-C5) hexon binding to the nuclear envelope and subsequent nuclear entry were dependent on Nup214, but not on Nup358 (Cassany et al., 2015). By immunoconfocal microscopy of HadV-D37 infected keratocytes with antibody against pericentrin, and as confirmed by electron microscopy, dynamin 2 knockdown led to repositioning of MTOCs closer to the nuclear envelope. This was associated with increased association of viral capsid with Nup358, correlating with data above showing that suppression of dynamin 2 expression increased nuclear entry of viral DNA, viral gene expression, and viral replication. Collectively, these results connect dynamin 2, microtubules, the MTOC, and nuclear delivery of adenoviral DNA.

Finally, we tested various dynamin 2 mutants to determine the sites specific to the effect of dynamin 2 on adenoviral trafficking in keratocytes. The dynamin 2 mutant Δ551-553, which is associated with Charcot-Marie-Tooth disease (Zuchner et al., 2005) and was previously shown to induce accumulation of acetylated, stable tubulin, and reduce transferrin trafficking but not transferrin endocytosis (Tanabe and Takei, 2009) appeared to increase viral gene expression, but the effect was not statistically significant. In contrast, the c-terminus mutant Δ746-786, which is deleted for the proline rich domain specific to binding of microtubules (Hamao et al., 2009), significantly increased viral gene expression. The K44A mutant, which eliminates dynamin 2 GTPase activity necessary for endocytosis but still binds microtubules, had no apparent effect on viral gene expression.

In summary, these data add clarity to existing models of adenovirus trafficking and infection. Our data is consistent with prior studies showing dynamin 2 is a negative regulator of microtubule acetylation and stability. We demonstrate herein an additional role for dynamin 2 in the control of MTOC localization. During natural infection, dynamin 2 appears to promote endosomal trafficking of adenovirus and innate immune responses to infection. Simultaneously, dynamin 2 serves to limit nuclear delivery of viral DNA, thus also restraining viral replication. Therefore, in keratocytes at least, dynamin 2 is effectively antiviral. It seems likely that the effect of dynamin 2 on viral trafficking and replication stems from complex synergisms and/or antagonisms between dynamin 2 influences on endosomal fission, microtubule instability, and actin polymerization, and perhaps other functions yet to be elucidated. However, initial viral entry into keratocytes did not appear to be affected in cells in which dynamin 2 function was either knocked down or increased. In contrast, the impact of dynamin 2 manipulation on the subsequent trafficking of virus was profound and correlated with microtubule dynamic instability.

Dynamin 2 plays significant roles in multiple cellular functions (Durieux et al., 2010), and its mutations have been implicated in important human neurologic disorders. Therefore, beyond its control of adenovirus trafficking, its novel influence on MTOC localization suggests important clues to the role of dynamin 2 in neurologic diseases. Furthermore, manipulation of MTOC localization through dynamin 2 could prove a useful strategy to improve delivery of transgenes in viral gene therapy.

4. Materials and methods

4.1. Antibodies and reagents

Anti-α-tubulin (1:5000, cat. no. T5168), anti-acetylated tubulin (0.05 μg/ml, cat. no. T7451), and chemicals, including cytochalasin D (cat. no. C8273), bafilomycin A1 (cat. no. 196000), nocodazole (cat. no. M1404) and streptolysin O (SLO; cat. no. S5265) were purchased from Sigma-Aldrich (Louise, MO). Antibodies to HA (1:5000, cat. no. AB9110), dynamin 2 (1:1000, cat. no. AB65556), and pericentrin (1:1000, cat. no. AB4448) were obtained from Abcam (Cambridge, MA). Anti-actin antibody (1:5000, cat. no. AM-4302) and EdU (5-ethynyl-2'-deoxyuridine) dye (cat. no. A10044) were obtained from Thermo Fisher Scientific (Waltham, MA). Anti-GM130 (1:1000, cat. no. 610822) was obtained from BD Transduction Laboratories (San Jose, CA). Antibodies to GAPDH (1:3000, cat. no. sc-322233) and Cy3 (1:200, cat. no. sc-166894) were obtained from Santa Cruz Biotechnology (Dallas, TX). Cy3 dye was obtained from GE Healthcare Life Sciences (Pittsburgh, PA, cat. no. PA23031). Lipofectamine® RNAiMAX ((Thermo Fisher Scientific, cat. no. 13778500)) and Lipofectamine® LTX Reagent with PLUS™ Reagent (cat. no. 15338030) were used for siRNAs transfection and plasmids transfection, respectively.

4.2. DNA constructs

Dynamin 2 expression was performed by cloning the dynamin 2 from a dynamin 2-expressing pmCherry N1 vector (Addgene, Cambridge, MA, cat. no. 27689) into pCAGGS-HA (Addgene, cat. no. 12438). For mutagenesis to generate K44A, the Q5 High-Fidelity DNA Polymerase (NEB, Ipswich, MA, cat. no. M0491S) was used according to the manufacturer's instructions. The Δ551-553 and Δ746-786 deletion mutants were generated by overlapping PCR. All mutants were confirmed by Sanger sequencing. For knockdown by siRNA, three regions of dynamin 2 were targeted and pooled. The scRNA control and siDNM2 were purchased from Integrated DNA Technologies (Coralville, IA).

4.3. Cell culture and viruses

Primary keratocytes were pooled from human donor corneas as previously described (Chodosh et al., 2000). After mechanical debridement of the corneal epithelium and endothelium, corneas were cut into 2 mm-diameter sections, and placed in individual wells of six-well Falcon tissue culture plates with DMEM supplemented with 10% FBS, penicillin G sodium, and streptomycin sulfate at 37 °C in 5% CO2. The fibroblast phenotype was authenticated by vimentin staining (data not shown). HAdV-D37 and A549 cells used in this study were purchased from American Type Culture Collection (ATCC, Manassas, VA, cat. nos. VR929 and CCL-185, respectively). All cells tested negative for endotoxin contamination by ToxinSensor chromogenic LAL (Limulus amebocyte lysate) endotoxin assay kit (GenScript, Piscataway, NJ, cat. no. L00350), and were mycoplasma negative by the Universal Mycoplasma Detection Kit (ATCC, Manassas, VA, cat. no. 30-1012K™). Virus purification was performed by cesium chloride gradient, and virus titered by the tissue culture infectious dose assay. Cy3-labeled virus was prepared as previously described (Leopold et al., 1998). For viral DNA labeling, A549 cells were grown with 10% FBS DMEM, washed in PBS, and infected with HAdV-D37 at high multiplicity in 5 ml of 2% FBS DMEM with EdU at a final concentration of 800 nM/ml. After 1 h incubation, 25 ml 2% FBS DMEM was added and the cells incubated for 7 days. EdU-incorporated virus was purified by CsCl gradient, as above. With or without pretreatment by transfection, cells grown to 90–100% confluence in six-well plates were washed in glucose-free DMEM with 2% FBS, and infected with purified HAdV-D37 at a multiplicity of infection (MOI) of 10 or mock-infected with virus-free dialysis buffer as a control. Virus infection was synchronized at 4 °C for 30 min, and the cells then washed using cold media. For virus internalization, pre-warmed media was added and cells were incubated for 2 h before Western blot or RNA isolation.

4.4. Transfections

Transfections were carried out using Lipofectamine® RNAiMAX reagent, following the manufacturers protocol. Briefly, 100 pmol DNM2 siRNA, or control, and 500 μl of Opti-MEM (Thermo Fisher Scientific) were mixed and then added to 5 μl of Lipofectamine® RNAiMAX. After 20 min incubation at room temperature, the transfection complex was added to cells at 60–80% confluence. For DNM2 overexpression, transfections were done using Lipofectamine LTX Reagent. 1.5 μg of plasmid DNA and 1.5 μl of PLUS™ Reagent was added to 500 μl of Opti-MEM Reduced Serum Medium, mixed and incubated at room temperature for 10 min 5 μl of Lipofectamine LTX Reagent was mixed with 500 μl of Opti-MEM Reduced Serum Medium and incubated for 10 min at room temperature. The diluted Lipofectamine LTX Reagent and diluted DNA were mixed and incubated at room temperature for 30 min, and added to the cells. After 5 h, media was changed to 10% FBS in DMEM. After 24 h post transfection, cells were serum starved in 2% FBS-DMEM media for 12 h. HAdV-D37 was added at a MOI of 10 for 1–2 h and the cells processed for confocal microscopy, Western blot, or qRT-PCR analysis.

4.5. Polymerase chain reaction

Total RNA was isolated by Direct-zol RNA MiniPrep Kit (Zymo Research, Irvine, CA, cat. no. R2060) according to the manufacturer's instructions. Contaminating genomic DNA was removed from the total RNA with Turbo DNA-free kit (Thermo Fisher Scientific, cat. no. AM 1907). Purity and quantity of the total RNA were determined using Nanodrop 2000C (Thermo Fisher Scientific). One μg of the total RNA isolated from each group was reverse transcribed to yield single stranded cDNA using 200 U Moloney Murine Leukemia Virus Reverse Transcriptase (M-MLV RTase, Promega, Madison, WI, cat. no. M1701), 10 mM dNTPs (Promega), 20 U of recombinant RNasin (Promega) and 100 ng of oligo(dT)15 (Integrated DNA Technologies) as primer in a total reaction volume of 20 μl. The reaction mix was incubated at 25°C for 5 min, then at 37°C for 1hr, followed by enzyme inactivation at 90 °C for 10 min. Primers for real-time, quantitative PCR were designed using Primer3 Plus (http://primer3plus.com/). Primer pairs used in these experiments are shown in Supplemental Table 2. A total of 1 μl of cDNA obtained by reverse transcription was used for qRT-PCR in a final volume of 20 μl containing 10 μl of 2× SYBR green master mix (Applied Biosystems, Foster City, CA) and 20 ng of specific forward and reverse primers each. RNA concentrations of samples were normalized using quantification of human GAPDH mRNA as the internal control. qRT-PCR was performed (StepOnePlusTM Real-Time PCR Systems; Life Technologies and Sequence Detection System; PE Applied Biosystems) with the cycling parameters: 95 °C for 10 min, 40 cycles of 95 °C for 10 s, 60 °C for 1 min, followed by final extension at 72 °C for 10 min, and dissociation curves were analyzed for generation of a single product. Relative transcript levels were calculated according to comparison between samples using the formula $2^{-\Delta\Delta Ct}$, where ΔΔCt equals ΔCt gene of interest – ΔCt experiment control.

To measure the effects of dynamin 2 on virion entry, cells were transfected with EV, OE-DNM2, scRNA or siDNM2. 24 h later, the cells were serum starved for 12 h in low-glucose DMEM containing 2% FBS, and after cell counting, washed in glucose-free DMEM containing 2% FBS and infected at a MOI of 1 for 30 min in 4°C, washed in cold medium twice and then incubated for 30 min at 37 °C. The cells were washed twice in PBS, then scraped for viral DNA isolation using the GeneJET Viral DNA/RNA Purification Kit (Thermo Fisher Scientific, cat. no. K0821) following the manufacturer's instruction as described

above. Conventional PCR was then performed at an initial 98 °C for 30 s, followed by 40 cycles of 98 °C (10 s), 60 °C (30 s) and 72 °C (15 s), and extension at 72 °C for 2 min. Results were confirmed to be in the linear range.

4.6. Immunoblot and Immunoprecipitation

Cells were lysed with chilled 1X cell lysis buffer (Cell Signaling Technology, Danvers, MA) containing 20 mM Tris, pH 7.5, 150 mM NaCl, 1 mM Na^2EDTA, 1 mM EGTA, 1% Triton X-100, 2.5 mM sodium pyrophosphate, 1 mM β-glycerophosphate, 1 mM Na_3VO_4, 1 μg/ml leupeptin plus 1 protease inhibitor (Sigma-Aldrich), and incubated at 4 °C for 5 min. Cell lysates were cleared by centrifugation at 14,000 × *g* for 10 min. The protein concentration of each supernatant was measured by BCA analysis (Thermo Fisher Scientific). Western blot and immunoprecipitation were performed in standard fashion. Blots were visualized with enhanced chemiluminescence (Thermo Fisher Scientific) using Kodak Image Station 4000R (Rochester, NY).

4.7. Streptolysin O assay

The assay was performed as described (Suomalainen et al., 2013) with minor modifications. A trypan blue exclusion assay was performed to assure the absence of cell toxicity while still permitting the SLO to permeabilize 80% of the total cell population within 5 min. The SLO concentration used in the assay was confirmed to maximally detect virus-labeled antibody by confocal microscopy. Briefly, Cy3-labeled HAdV-37 virus was bound to cells grown on glass coverslips at on ice for 30 min. Unbound virus was washed off, and the cells incubated in glucose free-DMEM medium at 37 °C. After 1 h incubation, the cells were washed twice with SLO binding buffer, and treated with SLO (Sigma Aldrich, St. Louis, MO), 0.4 μg/well on ice for 10 min. The unbound SLO was removed by washing, and cells in SLO binding buffer incubated at 37°C for 5 min. The cells were washed and incubated with anti-Cy3 mouse monoclonal antibody (Santa Cruz Biotechnology) on ice for 1 h. The cells were fixed on 3% paraformaldehyde, quenched to remove excess paraformaldehyde, and then permeabilized with 0.5% Triton-X 100 in PBS. Then the cells were blocked with 10% goat serum (Cell Signaling, Beverly, MA, cat. no. 5425S) in PBS at room temperature for 30 min, washed again with PBS, and incubated with rabbit anti-mouseIgG-Alexa Fluor 488 conjugate (Thermo Fisher Scientific, 1:500, cat. no. P11065) at room temperature for 45 min. The cells were stained with DAPI prior to confocal microscopy imaging. As an experimental control for SLO permeabilization, Cy3-labeled virus infected cells were fixed and permeabilized directly with 0.5% Triton X-100, without SLO treatment, and processed with anti-Cy3 antibody, followed by anti-mouse IgG-Alexa Fluor 488 conjugate as described above. To demonstrate SLO pore formation efficiency is not affected by different transfection conditions, cells were treated with SLO as above, were also incubated with the Golgi marker antibody anti-GM130 (1:1000), followed by rabbit anti-mouse IgG-Alexa Fluor 488 conjugate secondary antibody.

4.8. Confocal microscopy

Keratocytes grown on slide chambers (Nunc, Rochester, NY) were transfected with dynamin 2 siRNA, scRNA, dynamin 2 wild type, and empty vector constructs. After infection, cells were fixed in 4% formaldehyde for 10 min, washed in 2% FBS-PBS, and permeabilized in 0.1% Triton X-100 for 10 min. After 30 min blocking in 2% BSA-PBS, the cells were incubated in 1 mg/ml of specific antibody for 1 h at room temperature, washed, and incubated with secondary fluorescent antibody at the same concentration for 45 min at room temperature. Staining for EdU-incorporated HAdV-D37 DNA was carried out according to the manufacturer's protocol using the Click-iT® EdU Alexa Fluor® 488 Imaging Kit (Thermo Fisher Scientific, cat. no. C10337) for EdU-labeled HAdV-D37 detection. Cells were then washed and mounted using vectashield mounting medium (Vector Labs, Burlingame, CA) containing DAPI. Images were with a Leica SP5 confocal microscope using a 63x oil immersion objective. The images were scanned at 0.5 μm intervals, to obtain 15–20 Z-stacks per image, then constructed by maximum projection. For viral DNA quantification within individual nuclei, the central 5 Z-stacks of each image (nuclear stack) were chosen for analysis using Basic Intensity Quantification within ImageJ (https://imagej.nih.gov/ij/), with the Analyze Particles command. For analysis of the distance between pericentrin fluorescent signals and the nearest nuclear membrane, we applied the Leica Application Suite X, (LAS X, Leica Microsystems CMS GmbH).

4.9. Electron microscopy

Keratocytes grown on coverslips (Nunc) were transfected and infected. At 48 h post-transfection, cells were infected with purified HAdV-D37 virus at a MOI of 100 at 4 °C for 30 min, washed in media, and then warmed to 37 °C for 2 h. Cells were then fixed in 5% glutaraldehyde, 2.5% paraformaldehyde, and 0.06% picric acid in 0.2 M cacodylate buffer for 1 h, and post fixed in 1% osmium tetroxide (OsO4)/ 1.5% potassium ferrocyanide (KFeCN6) for 30 min, washed thrice in water, and incubated in 1% aqueous uranyl acetate for 30 min followed by 2 washes and subsequent dehydration in graded alcohol (5 min each; 50%, 70%, 95%, 2× 100%). Samples were embedded in plastic and polymerized at 60 °C. Ultrathin sections (~60 nm) were cut on a Reichert Ultracut-S microtome (Leica, Buffalo Grove, IL), placed on copper grids, stained with lead citrate, and examined in a JEOL 1200EX transmission electron microscope (Peabody, MA), and images were recorded with an AMT 2k CCD camera (Woburn, MA). Distance and virion location measurements were performed by a masked observer.

4.10. Cytokine array

At 24 h post transfection, cells were cultured in 2% FBS-DMEM media for 12 h. HAdV-D37 was added at a MOI of 10 at 4 °C for 30 min. The cells were then washed in media and warmed to 37 °C for 2 h. Cell supernatants were collected and processed for a cytokine expression assay (Human Cytokine Array, R&D, Minneapolis, MN, cat. no. ARY005B), with antibodies to 36 different proteins in duplicate on the array membranes. Array membranes were incubated for 60 min in 2 ml of blocking buffer on a shaker at room temperature. 500 μl of supernatant from each treatment group was incubated with 15 μl reconstituted human cytokine array detection cocktail for 60 min, and then placed on the array membranes overnight at 4 °C. Following a washing step, the membranes were incubated with a 1:2000 dilution of streptavidin-conjugated peroxidase for 45 min at room temperature. Proteins were detected by enhanced chemiluminescence (Amersham, Piscataway, NJ) and signals were captured, analyzed and normalized on a Kodak (Rochester, NY) Image Station 4000R for graphical representation. Each experiment was repeated at least three times.

4.11. Statistical analysis

Data was first checked for normality. Parametric data was analyzed by students *t*-test or ANOVA with Tukey testing. For nonparametric data, medians with interquartile ranges (IQR) were used, and the data analyzed by the Kruskal-Wallis test. $p < 0.05$ was considered statistically significant. All analyses were performed using GraphPad Prism v6.0 (GraphPad Software, San Diego, CA).

CRediT authorship contribution statement

Ji Sun Lee: Conceptualization, Data curation, Formal analysis, Investigation, Methodology, Validation, Writing - original draft. **Ashrafali M. Ismail:** Data curation, Methodology, Validation. **Jeong Yoon Lee:** Data curation. **Xiaohong Zhou:** Data curation. **Emma C. Materne:** Data curation. **James Chodosh:** Conceptualization, Formal analysis, Funding acquisition, Project administration, Resources, Writing - review & editing. **Jaya Rajaiya:** Conceptualization, Formal analysis, Funding acquisition, Investigation, Methodology, Project administration, Resources, Supervision, Validation, Visualization, Writing - original draft, Writing - review & editing.

Acknowledgements and financial disclosures

The authors gratefully acknowledge Maria Ericsson at the Conventional Electron Microscopy Facility, Harvard Medical School, for technical assistance. This work was supported by National Institutes of Health Grants EY013124, EY021558, and EY014104, Research to Prevent Blindness, Inc., New York, NY, The Falk Foundation, and the Massachusetts Lions Eye Research Fund. The funding organizations had no role in study design, data collection and analysis, decision to publish, or preparation of the manuscript.

Author contributions

Conceived and designed experiments: JR JC JSL. Performed experiments: JSL AMI JYL XZ JR. Analyzed the data: JR JC JSL. Wrote the paper: JSL JR JC.

Competing interests

None.

Appendix A. Supplementary material

Supplementary data associated with this article can be found in the online version at doi:10.1016/j.virol.2019.01.008.

References

Aleksandrowicz, P., Marzi, A., Biedenkopf, N., Beimforde, N., Becker, S., Hoenen, T., Feldmann, H., Schnittler, H.J., 2011. Ebola virus enters host cells by macropinocytosis and clathrin-mediated endocytosis. J. Infect. Dis. 204 (Suppl 3), S957–S967.

Al-Hasani, H., Hinck, C.S., Cushman, S.W., 1998. Endocytosis of the glucose transporter GLUT4 is mediated by the GTPase dynamin. J. Biol. Chem. 273, 17504–17510.

Asally, M., Yasuda, Y., Oka, M., Otsuka, S., Yoshimura, S.H., Takeyasu, K., Yoneda, Y., 2011. Nup358, a nucleoporin, functions as a key determinant of the nuclear pore complex structure remodeling during skeletal myogenesis. FEBS J. 278, 610–621.

Bailey, C.J., Crystal, R.G., Leopold, P.L., 2003. Association of adenovirus with the microtubule organizing center. J. Virol. 77, 13275–13287.

Basner-Tschakarjan, E., Gaffal, E., O'Keeffe, M., Tormo, D., Limmer, A., Wagner, H., Hochrein, H., Tuting, T., 2006. Adenovirus efficiently transduces plasmacytoid dendritic cells resulting in TLR9-dependent maturation and IFN-alpha production. J. Gene Med. 8, 1300–1306.

Belin, M.T., Boulanger, P., 1985. Cytoskeletal proteins associated with intracytoplasmic human adenovirus at an early stage of infection. Exp. Cell Res. 160, 356–370.

Boritz, E., Gerlach, J., Johnson, J.E., Rose, J.K., 1999. Replication-competent rhabdoviruses with human immunodeficiency virus type 1 coats and green fluorescent protein: entry by a pH-independent pathway. J. Virol. 73, 6937–6945.

Carter, G.C., Bernstone, L., Baskaran, D., James, W., 2011. HIV-1 infects macrophages by exploiting an endocytic route dependent on dynamin, Rac1 and Pak1. Virology 409, 234–250.

Cassany, A., Ragues, J., Guan, T., Begu, D., Wodrich, H., Kann, M., Nemerow, G.R., Gerace, L., 2015. Nuclear import of adenovirus DNA involves direct interaction of hexon with an N-terminal domain of the nucleoporin Nup214. J. Virol. 89, 1719–1730.

Chodosh, J., Astley, R.A., Butler, M.G., Kennedy, R.C., 2000. Adenovirus keratitis: a role for interleukin-8. Investig. Ophthalmol. Vis. Sci. 41, 783–789.

Dales, S., Chardonnet, Y., 1973. Early events in the interaction of adenoviruses with HeLa cells. IV. Association with microtubules and the nuclear pore complex during vectorial movement of the inoculum. Virology 56, 465–483.

De Camilli, P., Takei, K., McPherson, P.S., 1995. The function of dynamin in endocytosis. Curr. Opin. Neurobiol. 5, 559–565.

Doxsey, S.J., Stein, P., Evans, L., Calarco, P.D., Kirschner, M., 1994. Pericentrin, a highly conserved centrosome protein involved in microtubule organization. Cell 76, 639–650.

Durieux, A.C., Prudhon, B., Guicheney, P., Bitoun, M., 2010. Dynamin 2 and human diseases. J. Mol. Med. 88, 339–350.

Ferguson, S.M., De Camilli, P., 2012. Dynamin, a membrane-remodelling GTPase. Nat. Rev. Mol. Cell Biol. 13, 75–88.

Frampton Jr., A.R., Uchida, H., von Einem, J., Goins, W.F., Grandi, P., Cohen, J.B., Osterrieder, N., Glorioso, J.C., 2010. Equine herpesvirus type 1 (EHV-1) utilizes microtubules, dynein, and ROCK1 to productively infect cells. Vet. Microbiol. 141, 12–21.

Giovanni, A., Keramaris, E., Morris, E.J., Hou, S.T., O'Hare, M., Dyson, N., Robertson, G.S., Slack, R.S., Park, D.S., 2000. E2F1 mediates death of B-amyloid-treated cortical neurons in a manner independent of p53 and dependent on Bax and caspase 3. J. Biol. Chem. 275, 11553–11560.

Glotzer, J.B., Michou, A.I., Baker, A., Saltik, M., Cotten, M., 2001. Microtubule-independent motility and nuclear targeting of adenoviruses with fluorescently labeled genomes. J. Virol. 75, 2421–2434.

Gonzalez-Jamett, A.M., Momboisse, F., Haro-Acuna, V., Bevilacqua, J.A., Caviedes, P., Cardenas, A.M., 2013. Dynamin-2 function and dysfunction along the secretory pathway. Front. Endocrinol. 4, 126.

Hamao, K., Morita, M., Hosoya, H., 2009. New function of the proline rich domain in dynamin-2 to negatively regulate its interaction with microtubules in mammalian cells. Exp. Cell Res. 315, 1336–1345.

Haspot, F., Lavault, A., Sinzger, C., Laib Sampaio, K., Stierhof, Y.D., Pilet, P., Bressolette-Bodin, C., Halary, F., 2012. Human cytomegalovirus entry into dendritic cells occurs via a macropinocytosis-like pathway in a pH-independent and cholesterol-dependent manner. PLoS One 7, e34795.

Holla, P., Ahmad, I., Ahmed, Z., Jameel, S., 2015. Hepatitis E virus enters liver cells through a dynamin-2, clathrin and membrane cholesterol-dependent pathway. Traffic 16, 398–416.

Husain, M., Harrod, K.S., 2011. Enhanced acetylation of alpha-tubulin in influenza A virus infected epithelial cells. FEBS Lett. 585, 128–132.

Joseph, J., Tan, S.H., Karpova, T.S., McNally, J.G., Dasso, M., 2002. SUMO-1 targets RanGAP1 to kinetochores and mitotic spindles. J. Cell Biol. 156, 595–602.

Kamiyama, H., Kakoki, K., Yoshii, H., Iwao, M., Igawa, T., Sakai, H., Hayashi, H., Matsuyama, T., Yamamoto, N., Kubo, Y., 2011. Infection of XC cells by MLVs and Ebola virus is endosome-dependent but acidification-independent. PLoS One 6, e26180.

Kelkar, S.A., Pfister, K.K., Crystal, R.G., Leopold, P.L., 2004. Cytoplasmic dynein mediates adenovirus binding to microtubules. J. Virol. 78, 10122–10132.

Lee, B.K., Bhinge, A.A., Iyer, V.R., 2011. Wide-ranging functions of E2F4 in transcriptional activation and repression revealed by genome-wide analysis. Nucleic Acids Res. 39, 3558–3573.

Leopold, P.L., Ferris, B., Grinberg, I., Worgall, S., Hackett, N.R., Crystal, R.G., 1998. Fluorescent virions: dynamic tracking of the pathway of adenoviral gene transfer vectors in living cells. Hum. Gene Ther. 9, 367–378.

Leopold, P.L., Kreitzer, G., Miyazawa, N., Rempel, S., Pfister, K.K., Rodriguez-Boulan, E., Crystal, R.G., 2000. Dynein- and microtubule-mediated translocation of adenovirus serotype 5 occurs after endosomal lysis. Hum. Gene Ther. 11, 151–165.

Mabit, H., Nakano, M.Y., Prank, U., Saam, B., Dohner, K., Sodeik, B., Greber, U.F., 2002. Intact microtubules support adenovirus and herpes simplex virus infections. J. Virol. 76, 9962–9971.

Maeda, K., Nakata, T., Noda, Y., Sato-Yoshitake, R., Hirokawa, N., 1992. Interaction of dynamin with microtubules: its structure and GTPase activity investigated by using highly purified dynamin. Mol. Biol. Cell 3, 1181–1194.

Majhen, D., Calderon, H., Chandra, N., Fajardo, C.A., Rajan, A., Alemany, R., Custers, J., 2014. Adenovirus-based vaccines for fighting infectious diseases and cancer: progress in the field. Hum. Gene Ther. 25, 301–317.

Miles, B.D., Luftig, R.B., Weatherbee, J.A., Weihing, R.R., Weber, J., 1980. Quantitation of the interaction between adenovirus types 2 and 5 and microtubules inside infected cells. Virology 105, 265–269.

Mitchison, T., Kirschner, M., 1984a. Dynamic instability of microtubule growth. Nature 312, 237–242.

Mitchison, T., Kirschner, M., 1984b. Microtubule assembly nucleated by isolated centrosomes. Nature 312, 232–237.

Mulherkar, N., Raaben, M., de la Torre, J.C., Whelan, S.P., Chandran, K., 2011. The Ebola virus glycoprotein mediates entry via a non-classical dynamin-dependent macropinocytic pathway. Virology 419, 72–83.

Nakano, M.Y., Greber, U.F., 2000. Quantitative microscopy of fluorescent adenovirus entry. J. Struct. Biol. 129, 57–68.

Naranatt, P.P., Krishnan, H.H., Smith, M.S., Chandran, B., 2005. Kaposi's sarcoma-associated herpesvirus modulates microtubule dynamics via RhoA-GTP-diaphanous 2 signaling and utilizes the dynein motors to deliver its DNA to the nucleus. J. Virol. 79, 1191–1206.

Natarajan, K., Rajala, M.S., Chodosh, J., 2003. Corneal IL-8 expression following adenovirus infection is mediated by c-Src activation in human corneal fibroblasts. J. Immunol. 170, 6234–6243.

Nemerow, G.R., 2000. Cell receptors involved in adenovirus entry. Virology 274, 1–4.

Perreau, M., Welles, H.C., Pellaton, C., Gjoksi, B., Potin, L., Martin, R., Harari, A., Bett, A., Casimiro, D., Gall, J., Barouch, D.H., Kremer, E.J., Pantaleo, G., 2012. The number of Toll-like receptor 9-agonist motifs in the adenovirus genome correlates with induction of dendritic cell maturation by adenovirus immune complexes. J. Virol. 86,

6279–6285.
Pichler, A., Gast, A., Seeler, J.S., Dejean, A., Melchior, F., 2002. The nucleoporin RanBP2 has SUMO1 E3 ligase activity. Cell 108, 109–120.
Rajaiya, J., Sadeghi, N., Chodosh, J., 2009. Specific NFkappaB subunit activation and kinetics of cytokine induction in adenoviral keratitis. Mol. Vis. 15, 2879–2889.
Rajaiya, J., Zhou, X., Barequet, I., Gilmore, M.S., Chodosh, J., 2015. Novel model of innate immunity in corneal infection. Vitr. Cell Dev. Biol. Anim. 51, 827–834.
Salina, D., Enarson, P., Rattner, J.B., Burke, B., 2003. Nup358 integrates nuclear envelope breakdown with kinetochore assembly. J. Cell Biol. 162, 991–1001.
Salmon, E.D., Leslie, R.J., Saxton, W.M., Karow, M.L., McIntosh, J.R., 1984. Spindle microtubule dynamics in sea urchin embryos: analysis using a fluorescein-labeled tubulin and measurements of fluorescence redistribution after laser photobleaching. J. Cell Biol. 99, 2165–2174.
Scaife, R., Margolis, R.L., 1990. Biochemical and immunochemical analysis of rat brain dynamin interaction with microtubules and organelles in vivo and in vitro. J. Cell Biol. 111, 3023–3033.
Shajahan, A.N., Timblin, B.K., Sandoval, R., Tiruppathi, C., Malik, A.B., Minshall, R.D., 2004. Role of Src-induced dynamin-2 phosphorylation in caveolae-mediated endocytosis in endothelial cells. J. Biol. Chem. 279, 20392–20400.
Shpetner, H.S., Vallee, R.B., 1989. Identification of dynamin, a novel mechanochemical enzyme that mediates interactions between microtubules. Cell 59, 421–432.
Shpetner, H.S., Vallee, R.B., 1992. Dynamin is a GTPase stimulated to high levels of activity by microtubules. Nature 355, 733–735.
Shrivastava, N., Sripada, S., Kaur, J., Shah, P.S., Cecilia, D., 2011. Insights into the internalization and retrograde trafficking of Dengue 2 virus in BHK-21 cells. PLoS One 6, e25229.
Shtanko, O., Nikitina, R.A., Altuntas, C.Z., Chepurnov, A.A., Davey, R.A., 2014. Crimean-Congo hemorrhagic fever virus entry into host cells occurs through the multivesicular body and requires ESCRT regulators. PLoS Pathog. 10, e1004390.
Shurtleff, A.C., Nguyen, T.L., Kingery, D.A., Bavari, S., 2012. Therapeutics for filovirus infection: traditional approaches and progress towards in silico drug design. Expert Opin. Drug Discov. 7, 935–954.
Strunze, S., Engelke, M.F., Wang, I.H., Puntener, D., Boucke, K., Schleich, S., Way, M., Schoenenberger, P., Burckhardt, C.J., Greber, U.F., 2011. Kinesin-1-mediated capsid disassembly and disruption of the nuclear pore complex promote virus infection. Cell Host Microbe 10, 210–223.
Suomalainen, M., Nakano, M.Y., Keller, S., Boucke, K., Stidwill, R.P., Greber, U.F., 1999. Microtubule-dependent plus- and minus end-directed motilities are competing processes for nuclear targeting of adenovirus. J. Cell Biol. 144, 657–672.
Suomalainen, M., Nakano, M.Y., Boucke, K., Keller, S., Greber, U.F., 2001. Adenovirus-activated PKA and p38/MAPK pathways boost microtubule-mediated nuclear targeting of virus. EMBO J. 20, 1310–1319.
Suomalainen, M., Luisoni, S., Boucke, K., Bianchi, S., Engel, D.A., Greber, U.F., 2013. A direct and versatile assay measuring membrane penetration of adenovirus in single cells. J. Virol. 87, 12367–12379.
Takei, K., McPherson, P.S., Schmid, S.L., De Camilli, P., 1995. Tubular membrane invaginations coated by dynamin rings are induced by GTP-gamma S in nerve terminals. Nature 374, 186–190.
Tanabe, K., Takei, K., 2009. Dynamic instability of microtubules requires dynamin 2 and is impaired in a Charcot-Marie-Tooth mutant. J. Cell Biol. 185, 939–948.
Teigler, J.E., Kagan, J.C., Barouch, D.H., 2014. Late endosomal trafficking of alternative serotype adenovirus vaccine vectors augments antiviral innate immunity. J. Virol. 88, 10354–10363.
Thyberg, J., Moskalewski, S., 1999. Role of microtubules in the organization of the Golgi complex. Exp. Cell Res. 246, 263–279.
Valenzuela-Fernandez, A., Alvarez, S., Gordon-Alonso, M., Barrero, M., Ursa, A., Cabrero, J.R., Fernandez, G., Naranjo-Suarez, S., Yanez-Mo, M., Serrador, J.M., Munoz-Fernandez, M.A., Sanchez-Madrid, F., 2005. Histone deacetylase 6 regulates human immunodeficiency virus type 1 infection. Mol. Biol. Cell 16, 5445–5454.
de Vries, E., Tscherne, D.M., Wienholts, M.J., Cobos-Jimenez, V., Scholte, F., Garcia-Sastre, A., Rottier, P.J., de Haan, C.A., 2011. Dissection of the influenza A virus endocytic routes reveals macropinocytosis as an alternative entry pathway. PLoS Pathog. 7, e1001329.
Wang, I.H., Suomalainen, M., Andriasyan, V., Kilcher, S., Mercer, J., Neef, A., Luedtke, N.W., Greber, U.F., 2013. Tracking viral genomes in host cells at single-molecule resolution. Cell Host Microbe 14, 468–480.
Wang, I.H., Burckhardt, C.J., Yakimovich, A., Greber, U.F., 2018. Imaging, tracking and computational analyses of virus entry and egress with the cytoskeleton. Viruses 10.
Wenzel, P.L., Chong, J.L., Saenz-Robles, M.T., Ferrey, A., Hagan, J.P., Gomez, Y.M., Rajmohan, R., Sharma, N., Chen, H.Z., Pipas, J.M., Robinson, M.L., Leone, G., 2011. Cell proliferation in the absence of E2F1-3. Dev. Biol. 351, 35–45.
Xiao, J., Chodosh, J., 2005. JNK regulates MCP-1 expression in adenovirus type 19-infected human corneal fibroblasts. Investig. Ophthalmol. Vis. Sci. 46, 3777–3782.
Yousuf, M.A., Zhou, X., Mukherjee, S., Chintakuntlawar, A.V., Lee, J.Y., Ramke, M., Chodosh, J., Rajaiya, J., 2013. Caveolin-1 associated adenovirus entry into human corneal cells. PLoS One 8, e77462.
Zhong, M., Zheng, K., Chen, M., Xiang, Y., Jin, F., Ma, K., Qiu, X., Wang, Q., Peng, T., Kitazato, K., Wang, Y., 2014. Heat-shock protein 90 promotes nuclear transport of herpes simplex virus 1 capsid protein by interacting with acetylated tubulin. PLoS One 9, e99425.
Zuchner, S., Noureddine, M., Kennerson, M., Verhoeven, K., Claeys, K., De Jonghe, P., Merory, J., Oliveira, S.A., Speer, M.C., Stenger, J.E., Walizada, G., Zhu, D., Pericak-Vance, M.A., Nicholson, G., Timmerman, V., Vance, J.M., 2005. Mutations in the pleckstrin homology domain of dynamin 2 cause dominant intermediate Charcot-Marie-Tooth disease. Nat. Genet. 37, 289–294.